nanomaterials

MDPI

Article

Bi_2WO_6/C-dots/TiO_2: A novel z-scheme photocatalyst for the degradation of fluoroquinolone levofloxacin from aqueous medium

Shelja Sharma[1], Alex O. Ibhadon[2], M. Grazia Francesconi[3], Surinder Kumar Mehta[4], Sasikumar Elumalai[1], Sushil Kumar Kansal[5]*, Ahmad Umar[6]*and S. Baskoutas[7]

[1] Centre of Innovative and Applied Bioprocessing, Mohali-140306, India, sshhelja@yahoo.in (S.S.); sasikumar@ciab.res.in (S.E.)
[2] Department of Chemical Engineering, The University of Hull, Hull HU6 7RX, United Kingdom; a.o.ibhadon@hull.ac.uk (A.O.I.)
[3] Department of Chemistry, University of Hull, Hull HU6 7RX, United Kingdom; m.g.francesconi@hull.ac.uk (M.G.F.)
[4] Department of Chemistry and Centre of Advanced Studies, Panjab University, Chandigarh 160014, India; skmehta@pu.ac.in (S.K. M.)
[5] Dr. S.S. Bhatnagar University Institute of Chemical Engineering and Technology, Panjab University, Chandigarh 160014, India; sushilkk1@yahoo.co.in (S.K.K.)
[6] Department of Chemistry, Faculty of Science and Arts, Promising Centre for Sensors and Electronic Devices (PCSED), Najran University, Najran-11001, Kingdom of Saudi Arabia; ahmadumar786@gmail.com (A.U.)
[7] Department of Materials Science, University of Patras, Greece; bask@upatras.gr (S.B.)
* Correspondence: sushilkk1@pu.ac.in (S.K.K.), ahmadumar786@gmail.com (A.U.)

Received: date; Accepted: date; Published: date

Abstract: Photocatalytic materials and semiconductors of appropriate structural and morphological architectures as well as energy band gaps are the materials needed for mitigating current environmental problems as these materials have the ability to exploit the full spectrum of solar light in a number of applications. Hence, constructing a Z-scheme heterojunction is an ideal approach to overcome the limitations of a single component or traditional heterogeneous catalysts for the competent removal of organic chemicals present in wastewater, to mention one of the areas of application. A Z-scheme catalyst possesses many attributes, including enhanced light harvesting capacity, strong redox ability and different oxidation and reduction positions. In the present work, a novel ternary z-scheme photocatalyst, i.e. Bi_2WO_6/C-dots/TiO_2, has been prepared by a facile chemical wet technique. The prepared solar light driven z-scheme composite was characterized by many analytical and spectroscopic practices including powder X-ray diffraction (XRD), field emission scanning electron microscopy (FE-SEM), N_2 adsorption-desorption isotherm, Fourier-transform infrared spectroscopy (FT-IR), photoluminescence (PL) and UV-vis diffuse reflectance spectroscopy (DRS). The photocatalytic activity of the Bi_2WO_6/C-dots/TiO_2 composite was evaluated by studying the degradation of fluoroquinolone drug, levofloxacin under solar light irradiation. Almost complete (99%) decomposition of the levofloxacin drug was observed in 90 minutes of sunlight irradiation. The effect of catalyst loading, initial substrate concentration and pH of the reaction was also optimized. The photocatalytic activity of the prepared catalyst was also compared with that of bare Bi_2WO_6, TiO_2 and TiO_2/C-dots under optimized conditions. Scavenger radical trap studies and terephthalic acid (TPA) fluorescence technique were done to understand the role of the photoinduced active radical ions that are bring about the decomposition of levofloxacin. Based on these studies, the plausible degradation trail of levofloxacin was proposed and was further supported by LC-MS analysis.

Keywords: Bi_2WO_6/C-dots/TiO_2; Z-scheme, photocatalysis; levofloxacin; LC-MS; degradation pathways

1. Introduction

The occurrence of pharmaceuticals and personal care products (PPCPs) in environmental samples has been observed over the past few decades and these compounds are now considered as contaminants of emerging concern as these are biologically active even at low concentrations [1,2]. Pharmaceuticals have appeared as rapidly growing environmental contaminants and are one of the major concerns of national public health experts [3]. Hence, these substances have been called "pseudo-persistent" pollutants due to their unregulated and continuous discharge directly or indirectly to r water systems via number of ways [4]. A large amount of these compounds enter water bodies primarily from wastewater treatment plant effluents and other sources such as hospital discharge, inappropriate disposal by manufacturer and from expired and unused drugs [5]. Local release of pharmaceutical drugs may cause problems in aquatic environments since they are active at low concentrations ranging from ng/L-μg/L [6]. However, the consumption of few drugs is shockingly high. For instance, the antibiotics, the defined daily dose is quite high as compared to the dose defined by World Health Organization [7]. Levofloxacin is such an example of a broad spectrum fluoroquinolone antibiotic which is widely used as an antibacterial agent [8]. The high consumption of fluoroquinolones drug and its poor disposal into water sources has resulted in a generation of more toxic and resistant fecal bacteria [9]. Conventional wastewater treatment plants are not designed for the complete elimination of these compounds owing to their resistance to biodegradation. P photocatalysis technique has emerged as promising technology and has garnered increased research attention [10,11]. Photocatalysts with broad absorption range, narrow band gap, high stability, efficient charge separation, high redox abilities can directly convert solar energy into storable energy compounds and degrade hazardous organic pollutants into least toxic compounds. Photocatalysts can also reduce CO_2 to renewable fuels, such as ---?? [12-16]. However, a single photocatalyst cannot possess all the ideal characteristics, for example, wide absorption range and strong redox abilities are difficult to achieve simultaneously in a single photocatalyst [17]. These properties can be achieved by designing appropriate photocatalytic systems. In a heterojunction type photocatalytic system, two photocatalysts of dissimilar band gap values are involved, the photo-induced electrons from the conduction band (CB) of one photocatalyst (PC1) migrates to the CB of other photocatalyst (PC2) and photo-induced holes also migrate from the valence band (VB) of PC2 to VB of PC1, thereby leading to increased charge separation and reduced recombination of charge carriers. However, the redox capabilities of both photocatalysts are neglected as the oxidation and reduction processes are occurring on the semiconductors with the lower oxidation and reduction potentials, respectively. Hence, even if this heterogeneous photocatalytic system can hinder the recombination of photogenerated charge carriers, it cannot possess efficient charge separation and the strong redox ability simultaneously [18,19]. To address these limitations calls an investigation of more efficient a photocatalytic systems.

Artificial Z-scheme photocatalytic system can overcome the drawbacks associated with single component and heterojunction type photocatalyst systems. It mimics the photosynthesis process that includes a two-step photoexcitation. Like a heterojunction type photocatalytic system, it can also efficiently overcome the recombination of photogenerated charge carriers although in this case, strong redox abilities can also be achieved by combining two narrow band gap semiconductors. In the typical mechanism, the photogenerated electrons on CB of PCI do not migrate to PCII, making PCI electron rich region and thereby, obstruct the photo-oxidation of PCI and simultaneously making PCII a hole rich region which can cover PCII from photo-oxidation [20,21]. So, in the present work, a ternary z-scheme photocatalyst, (Bi_2WO_6/C-dots/TiO_2), was synthesized by a facile surfactant free hydrothermal method. The synthesized catalyst was characterized by analytical and spectroscopic techniques and, further, its photocatalytic activity was tested against the decomposition of the antibiotic levofloxacin under sunlight.

2. Materials and Methods

L-ascorbic acid ($C_6H_8O_6$, < 99.0%), bismuth (III) nitrate pentahydrate ($Bi(NO_3)_3.5H_2O$, 98.0%), sodium tungsten oxide dihydrate ($Na_2WO_4.2H_2O$, 95.0%) and ethanol (C_2H_5OH) were bought from Alfa Aesar, United Kingdom, respectively. Terephthalic acid (TPA) ($C_8H_6O_4$, 99.0%), sodium hydroxide (NaOH, 99.0%), formic acid (HCOOH, 99.0%), potassium iodide (KI, 99.0%) and titanium isopropoxide (TTIP, <99.0%) and were purchased from Sigma-Aldrich, India. bought from Merck, India. Fluoroquinolone drug levofloxacin was procured from Saurav Chemicals, Derabassi, India. Deionized water has been utilized for all experiments.

2.2. Preparation of the catalysts

2.2.1 Synthesis of Bi_2WO_6

Bi_2WO_6 was synthesized by the hydrothermal method. In a brief process, 0.006 mol (1.455 g) of bismuth nitrate pentahydrate ($Bi(NO_3)_3.5H_2O$) was solubilized in 37.5 mL of water, labelled as solution 1. 0.003 mol (0.5 g) of sodium tungstate dihydrate ($Na_2(WO_4).2H_2O$) was dissolved in 12.5 mL of ethylene glycol and labelled as solution 2. The latter was introduced into former under sonication with drop wise addition. The resultant sol was stirred for an hour and then transferred to a 75 mL Teflon-lined stainless steel autoclave for hydrothermal treatment at 160^0C for 25 h. After the reaction, the precipitates were collected via centrifugation and washed with ethanol and water thoroughly and dried at 50^0C overnight.

2.2.2 Synthesis of TiO_2/C-dots

TiO_2 was synthesized by hydrothermal method with slight modifications from the previous work [22]. In this procedure, 6 mL of TTIP was added to 10 mL of ethanol and the mixture was stirred for 30 minutes and designated as solution 1. Further, the equimolar concentrations of water and ethanol solution (50 mL) and named as solution 2. Solution 2 was introduced into solution 1 slowly with constant stirring for 30 minutes. Immediate turbidity was seen in the solution after the addition. The turbid solution was then placed in Teflon lined stainless steel autoclave. Meanwhile, L-ascorbic acid (0.5 g), was dissolved into 50 mL of ethanol and kept under stirring and then it was transferred into the Teflon autoclave for hydrothermal treatment at 180^0C for 4 h. The obtained precipitates were separated by centrifugation after the completion of hydrothermal reaction. The precipitates were carefully washed with the water and ethanol and kept for drying in oven at 60^0C. The colour of powder changed from clear white to pale white, specifying the successful synthesis of TiO_2/C-dots.

2.2.3 Synthesis of Bi_2WO_6/C-dots/TiO_2

Bismuth tungstate (0.5 g) and TiO_2/C-dots (0.25 g) were dispersed in 25 mL of ethanol and kept under magnetic stirring overnight. The precipitates collected were then washed, filtered and dried at 50^0C overnight.

2.3 Characterizations of prepared catalysts

The crystallinity and structure analysis of the catalysts were determined by Powder X-ray diffraction using a PANalytical Empyrean X-ray diffractometer with Cu $K_{\alpha 1}$ radiation. Results were recorded using the instruments inbuilt software. The XRD patterns obtained were analysed using PANalytical Highscore Plus. Fourier Transformation Infra-red of the powder samples were recorded on Thermo Scientific Nicolet iS5 FTIR spectrometer (wavenumber range: 600-4000 cm^{-1}). The surface morphology of the samples was analyzed using the Hitachi-SU8010 field-emission electron microscope (FE-SEM), operating at the voltage of 15 kV equipped with energy dispersive spectroscopy (EDS; Bruker XFlash). The thermogravimetric analysis (TGA) of the catalysts was performed on Perkin Elmer Simultaneous Thermal Analyzer (STA) 8000 in the temperature range30^0C to 800^0C. The fluorescence

spectra of the samples were recorded on Cary Eclipse Fluorescence Spectrophotometer (Agilent Technologies). The UV-vis DRS spectra of the photocatalysts were obtained from Shimadzu UV-2600 spectrophotometer with barium sulphate taken as a reference. The nitrogen adsorption and desorption isotherms of the prepared catalyst were measured using surface area analyser BELSORP, prior to the analysis, the samples were degassed at 100^0C for 24 hours. The pore size distribution curve, total pore volume and mean pore diameter were determined from the desorption branch of Barrett- Joyner- Halenda (BJH) model. The absorbance of the samples was recorded on the Shimadzu UV-Vis spectrophotometer (UV-2600). The liquid chromatography–mass spectroscopy (LC-MS) of the drug samples was analysed on Agilent Technologies 6120 Quadrupole LC-MS to determine the degradation products formed and other intermediates.

2.4 Photocatalytic experiments

The photocatalytic experiments were carried out using antibiotic drug levofloxacin as a target pollutant and its degradation was observed under direct sunlight irradiation. The solar experiments were carried out under direct sunlight in a cylindrical slurry batch reactor with the average intensity of 70 Klux. In a typical photocatalytic test, different amounts of prepared photocatalyst was introduced in levofloxacin solution (100 mL, 10 mg/L) and kept under stirring in dark for 30 minutes for the achievement of adsorption-desorption process. The reaction solution was then subjected to solar light irradiation. The samples (2 mL) were drawn from the reaction at set time periods and made to pass via 0.22 μm Millex syringe filter. Other process parameters, i.e. catalyst dosage, pH and initial pollutant concentration were studied for the photocatalytic experiments. The % degradation can be determined from the equation given below:

$$\textbf{\% degradation} = \frac{C_0 - C}{C}\ \boldsymbol{X}\ \mathbf{100}$$

Where C_0 and C are the initial drug concentration and concentration of drug at time t.

2.5 Investigation of function of active radical ions in the decomposition of levofloxacin under sunlight illumination

The generation of hydroxyl radicals from the sunlight illuminated Bi_2WO_6/C-dots/TiO_2 was examined using a TPA fluorescence technique. The levofloxacin drug solution was replaced with 100 mL of 0.5 mM TPA solution in 2 mM sodium hydroxide. The optimized dose of photocatalyst was added into the TPA solution and illuminated by direct sunlight under constant stirring and the samples were drawn from the respective solutions at pre-designed intervals. The aliquots were then made to pass through filter and the corresponding fluorescence spectra were obtained from PL spectrophotometer at λ_{ex}=315 nm. Further, scavenger experiments were implemented to investigate the occurrence and character of active radical ions in the photocatalytic system. Potassium iodide (KI) and formic acid (HCOOH) of concentrations 0.01 M, were served as scavenger for holes (h^+) and electrons (e^-) in the reaction system. The quenchers were dispersed into the levofloxacin drug solution before the adding the catalyst and solar light illumination maintaining other optimized parameters constant, i.e., drug concentration, catalyst dose and pH of drug solution.

3. Results and discussion

3.1 Characterization of the synthesized catalysts

The crystallinity, structural characteristics and purity analysis were studied by powder XRD technique. The powder XRD patterns of Bi_2WO_6, TiO_2/C-dots and Bi_2WO_6/C-dots/TiO_2 are displayed in Fig. 1. In the case of TiO_2/C-dots, the well-known and sharp peaks at 2θ = 25.4, 38.10, 48.05, 53.80, 55.11 and 62.81 were observed, that are corresponding to the pure anatase phase of TiO_2, and the results were found to be in consistence with JCPDS card no. 21-1272 [22,23]. It was clear from the figure that no distinctive peak for C-dots around 20^0-24^0 was observed in the pattern which might be

due to reduced concentration of C-dots. The values of lattice constants ''a'' and ''c'' were 3.78 Å and 9.44 Å, calculated from tetragonal crystal. In case of Bi_2WO_6, the diffraction peaks centered at 2θ= 28.30°, 32.81°, 35.90°, 47.12°, 55.81°, 58.52°, 68.90°, 76.0° and 78.3° are attributed to the orthorhombic phase of Bi_2WO_6 and are in agreement with JCPDS card No. 39-0256 [24-27]. The values of lattice constants of Bi_2WO_6 were computed to be 5.456 Å (a), 5.454 Å (b) and 16.455 Å (c). In the XRD pattern of Bi_2WO_6/C-dots/TiO_2, all the peaks belonging to Bi_2WO_6 and TiO_2/C-dots were present, thereby confirming the successful synthesis of z-scheme catalyst. Narrow and sharp diffraction patterns confirmed the crystalline nature of the composite. The average crystallite size of the z-scheme photocatalyst was computed from Debye-Scherrer's formula as given:

$$D=0.94\lambda/\beta\cos\theta$$

Where D is the crystallite size (average), λ is the wavelength of X-ray radiation, β is the broadening of the diffraction line assessed at full width half maxima value (FWHM) and θ is the Bragg's angle. The crystallite size of the z-scheme catalyst (Bi_2WO_6/C-dots/TiO_2) was computed to be 34.29 nm.

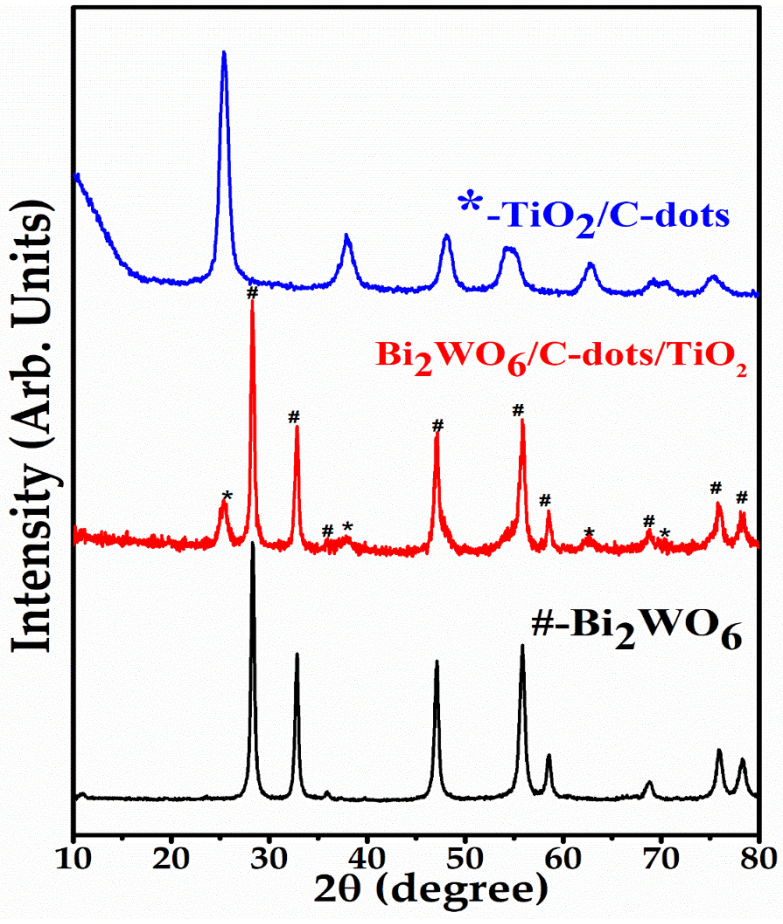

Fig. 1. XRD spectra of Bi_2WO_6 (#), TiO_2/C-dots (*), and Bi_2WO_6/C-dots/TiO_2.

The morphologies of Bi_2WO_6 and Bi_2WO_6/C-dots/TiO_2 were depicted with FESEM provided with EDS. Fig. 2 displays the FESEM and EDS analysis of Bi_2WO_6/C-dots/TiO_2 z-scheme nano-photocatalyst. In Fig. 2a, it can be seen that Bi_2WO_6 exhibited flakes like morphology of irregular size.

The edges of flakes were found to be asymmetrical and uneven, however the base and sides were found to be smooth (Fig. 2b).

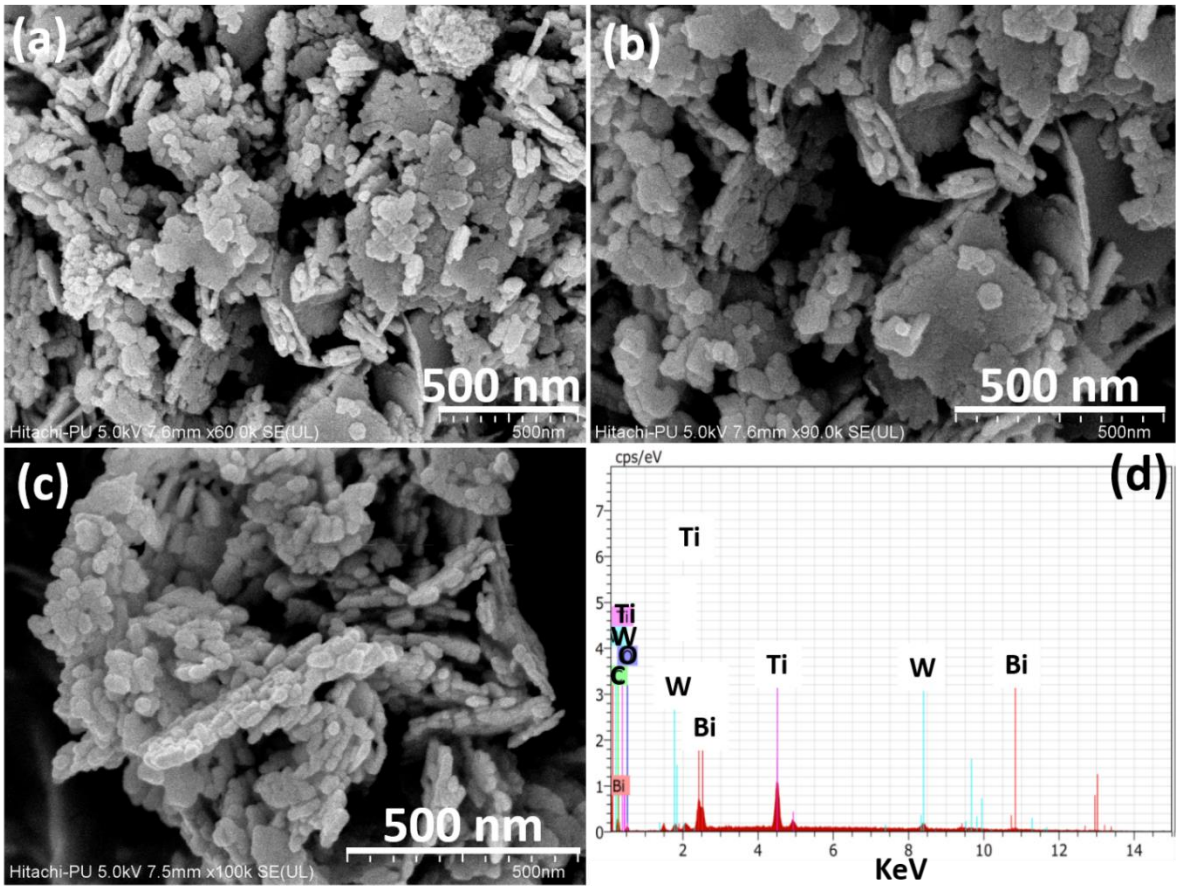

Fig. 2. (a-c) FESEM images of Bi_2WO_6/C-dots/TiO_2 at different magnifications. (d) EDX of Bi_2WO_6/C-dots/TiO_2

The nanoflakes were grown in high density and these were clustered together with each other in random fashion exhibiting high aspect ratio (Fig. 2c), whereas the nanoparticles of the TiO_2/C-dots were embedded at the surface of flakes. EDS spectrum of Bi_2WO_6/C-dots/TiO_2 displayed the presence of bismuth (Bi), titanium (Ti), tungstate (W), carbon (C) and oxygen (O) in the photocatalyst (Fig. 2d). The morphology of Bi_2WO_6 and TiO_2/C-dots was also studied, Bi_2WO_6 also possessed nanoflakes morphology but the flakes were highly agglomerated in nature (Fig. S1 and S2). EDS spectrum of Bi_2WO_6 is given in supplementary information (Fig. S1) and its elemental composition is depicted in Table S1.

Table 1. Elemental composition of Bi_2WO_6/C-dots/TiO_2

Element	Series	unn. C [wt.%]	norm. C [wt.%]	Atom. C [wt.%]	Error (3 Sigma) [wt.%]
Bismuth	M-Series	17.10	14.74	5.10	1.98
Carbon	K-Series	6.61	5.70	34.33	4.22
Oxygen	K-Series	1.45	1.25	5.65	1.47
Tungsten	L-Series	65.80	56.73	22.32	7.86
Titanium	K-Series	25.03	21.58	32.60	2.37

	Total	115.99	100.00	100.00	

Further, the synthesis of z-scheme catalyst (Bi_2WO_6/C-dots/TiO_2) was also confirmed by elemental mapping as shown in Fig. 3. The mapping outcomes concluded that elements concerned i.e., Bi, Ti, W and C and O were present in various proportions and quantity in the catalyst In summary, there was inhomogeneous contribution of elements in the catalyst carrier material. The elemental composition from EDS spectrum of sample is displayed in Table 1.

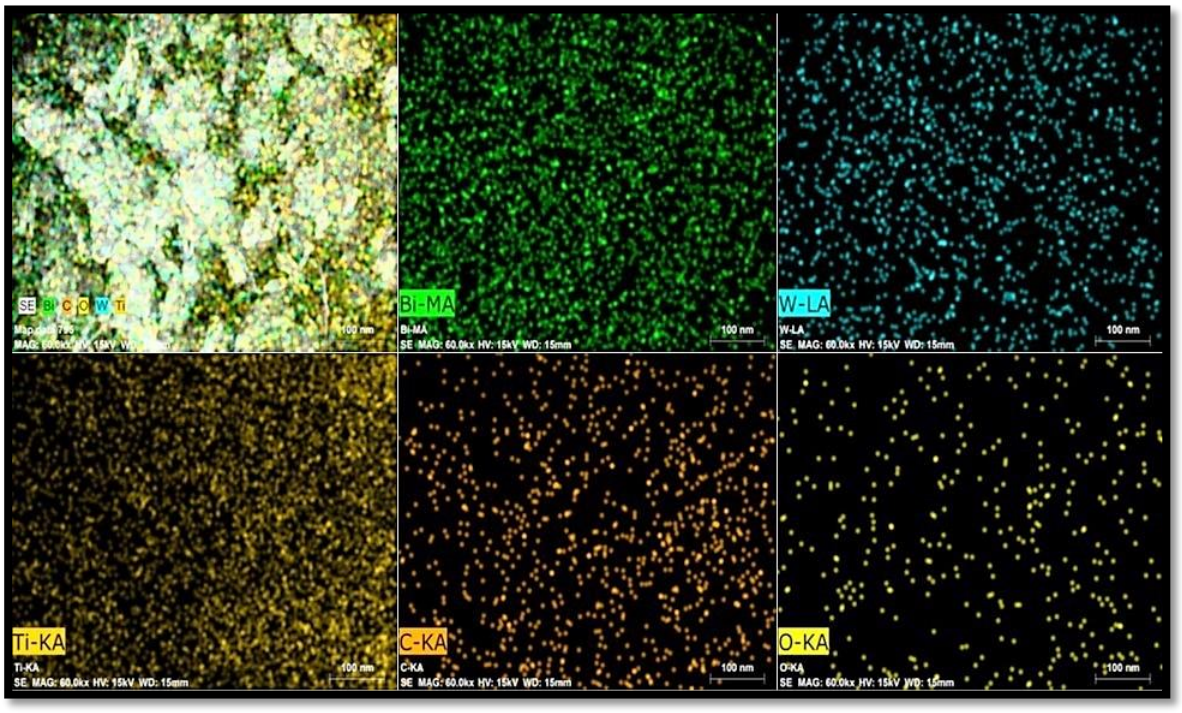

Fig. 3 Elemental mapping of Bi_2WO_6/C-dots/TiO_2 showing different colours for Bi, W, Ti, C and O

FTIR spectroscopy revealed the presence of functional groups and other chemical composition of catalyst as shown in Fig 4a. The broad absorption curve in the region 3000-3400 cm^{-1} and sharp peak at 1620 cm^{-1} might be related to the bending and stretching modes of adsorbed water on the surface of catalyst [28,29]. The distinctive bands between 600–1000 cm^{-1} were attributed to W-O bond in terms of stretching and bridging modes. For instance, W-O stretching vibration was positioned at 682 cm^{-1} and W-O-W bending vibrations modes were centered at 821 cm^{-1} and 1290 cm^{-1} [30,31]. Thermogravimetric analysis of Bi_2WO_6/C-dots/TiO_2 and TiO_2/C-dots presented the thermal properties of the synthesized catalysts (Fig. 4b). It was noticed that TiO_2/C-dots showed 22.8% weight loss (initial weight: 3.506 g, weight loss: 0.8 g), whereas Bi_2WO_6/C-dots/TiO_2 exhibited only 7.73% weight loss (initial weight: 4.306 g, weight loss: 0.33 g), in the temperature ranging from 30^0C to 800^0C. The weight loss in both the cases was because of the desorption of adsorbed water from the surface of the catalysts and degradation of oxygen containing functional groups from the surface [32]. The z-scheme nano-photocatalyst exhibited exceptionally high thermal stability throughout the whole temperature range.

The optical characteristics of the synthesized z-scheme nanophotocatalyst were studied using the PL and UV-vis DRS. PL emission is directly related to the efficient separation of photoinduced charge transporters. PL spectra of Bi_2WO_6 and Bi_2WO_6/C-dots/ TiO_2 were obtained at an excitation

wavelength of 360 nm (Fig. 4c). Bi_2WO_6 exhibited sharp peak at 421 nm ascribed to the higher probabilities of recombination of photoinduced charge transporters. Few PL emission bands in the wavelength area 450-500 nm were related to the blue-green emission band. On the other hand, in Bi_2WO_6/C-dots/TiO_2, the PL intensity of sharp peak at 421 nm also got reduced, implying that there would be lesser recombination of photoinduced charge carriers. The outcome suggested that greater number of induced charge carriers would be available to participate in the photocatalytic mechanism. A broad and minor peak at 525 nm are related to metal atom/crystal defects owing to oxygen vacancies [33,34]. The absorption properties and band gap of Bi_2WO_6 and Bi_2WO_6/C-dots/TiO_2 were determined by UV-vis DRS (Fig. 4d). The energy band gap of Bi_2WO_6 and Bi_2WO_6/C-dots/TiO_2 was calculated using the equation below:

$$E_g = \frac{1240}{\lambda_{max}}$$

where E_g is the calculated energy band gap (eV) and λ_{max} is the observed wavelength calculated from the edge of absorption curve by drawing a tangent to it .

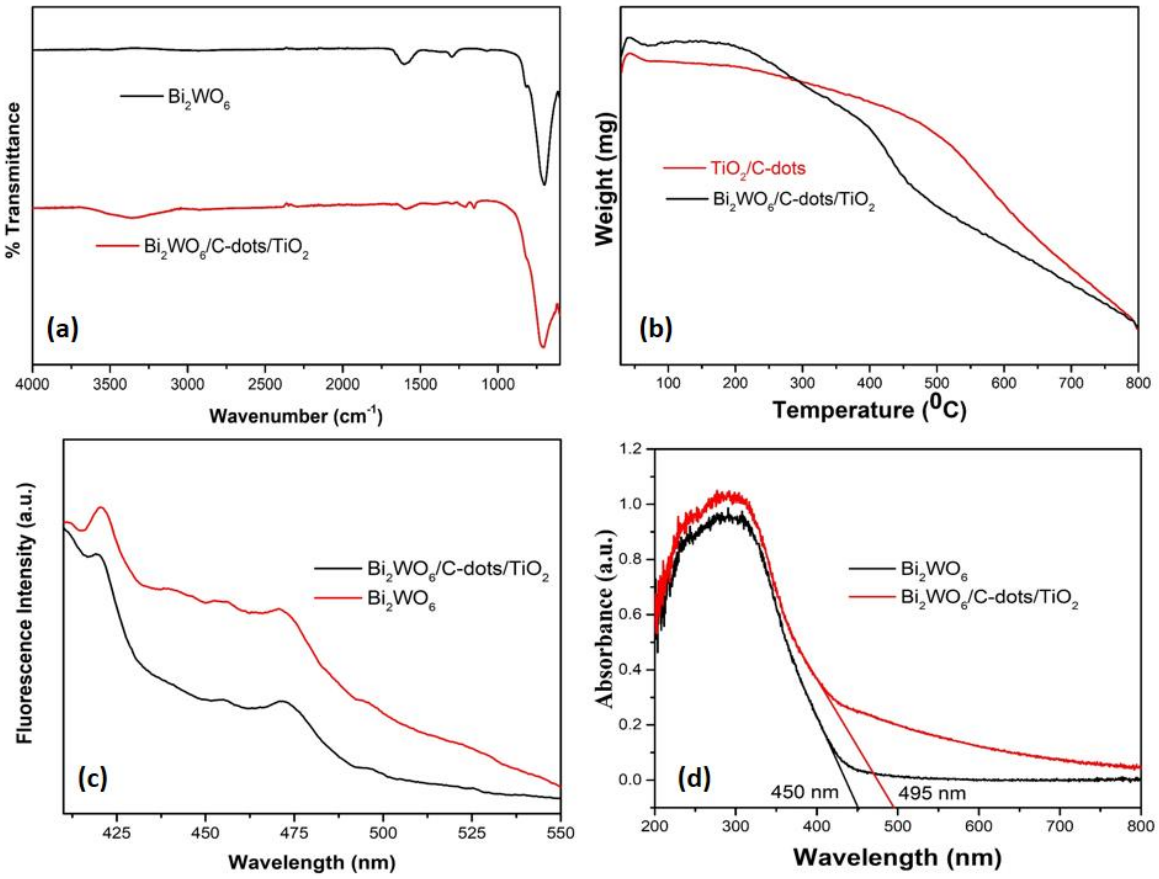

Fig. 4 FTIR analysis of Bi_2WO_6 and Bi_2WO_6/C-dots/TiO_2 (b) Thermogravimetric analysis of TiO_2/C-dots and Bi_2WO_6/C-dots/TiO_2 (c) PL spectra of Bi_2WO_6 and Bi_2WO_6/C-dots/TiO_2 at λ_{ex}= 360 nm (d) UV-vis DRS analysis of Bi_2WO_6 and Bi_2WO_6/C-dots/TiO_2.

The maximum absorption edges of Bi_2WO_6 and Bi_2WO_6/C-dots/TiO_2 were observed at the 450 nm and 495 nm, and the corresponding values of E_g were estimated to be 2.75 eV and 2.50 eV. The lower value of the E_g indicated the enhanced light absorption ability of the Bi_2WO_6/C-dots/TiO_2 and

similar for the photocatalytic degradation of levofloxacin by Bi_2WO_6/C-dots/TiO_2 [33]. PL studies also supported the improved degradation of levofloxacin by Bi_2WO_6/C-dots/TiO_2 under direct sunlight.

The specific surface area of the composite gives an idea about the accessibility of active sites on the surface of catalyst, more the specific surface area of the catalyst, the more will be improvement in the charge movement of photoinduced charge carriers hence, enhanced photocatalytic activity. Brunauer–Emmett–Teller (BET) results measure the surface area of porous materials. N_2 adsorption-desorption isotherm and BJH pore size distribution curve of the synthesized Bi_2WO_6 and Bi_2WO_6/C-dots/TiO_2 z-scheme catalyst are shown in Fig. 5. The hysteresis loop for both Bi_2WO_6 and Bi_2WO_6/C-dots/TiO_2 z-scheme catalyst was of type-IV isotherm, representing typical mesoporous nature of nanostructures. The specific surface area of Bi_2WO_6 and Bi_2WO_6/C-dots/TiO_2 was determined to be 18.364 m^2/g and 48.8 m^2/g, respectively and total pore volume of Bi_2WO_6 and Bi_2WO_6/C-dots/TiO_2 was computed to be 0.0309 cm^3/g and 0.102 cm^3/g, respectively. Hence, the increased specific surface area of the z-scheme catalyst, i.e. Bi_2WO_6/C-dots/TiO_2 over bare Bi_2WO_6 also promise its enhanced degradation of levofloxacin drug under sunlight illumination.

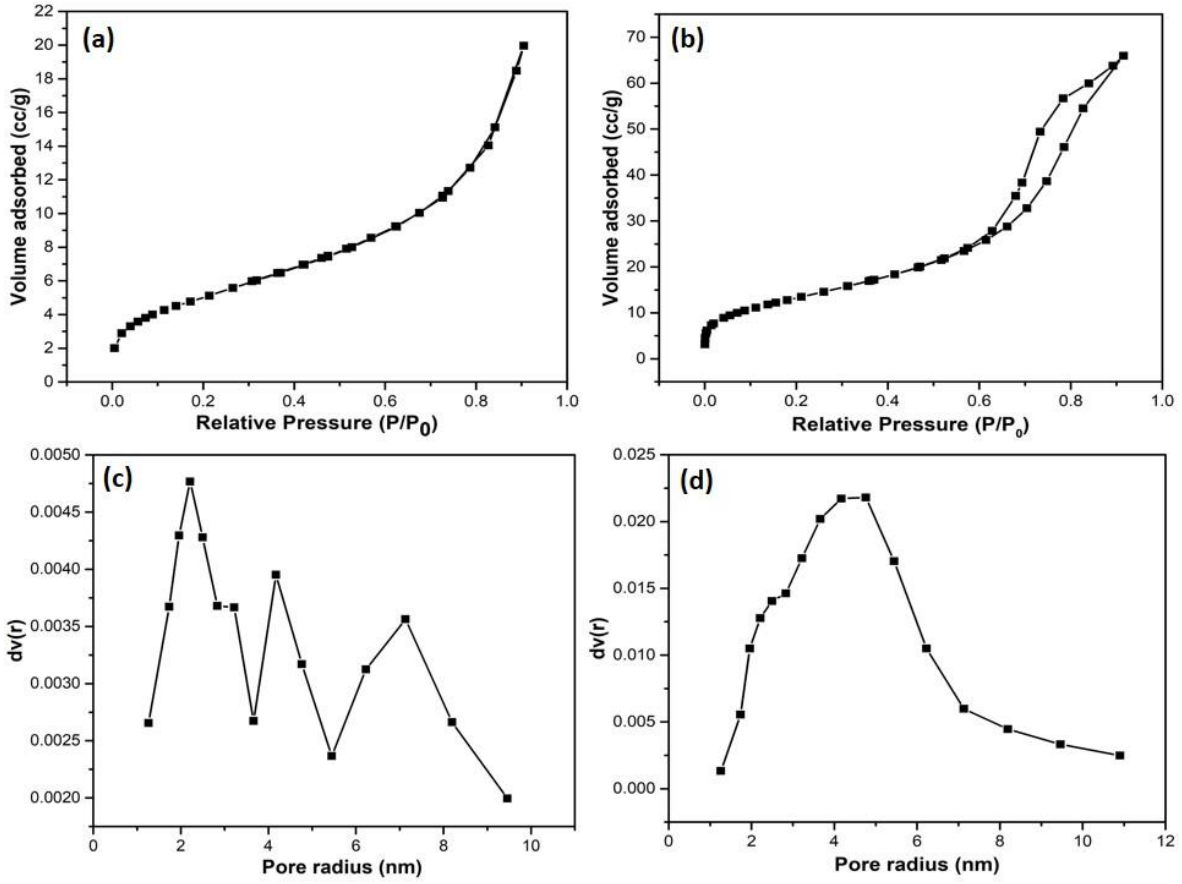

Fig. 5 N_2 adsorption-desorption isotherm of (a) Bi_2WO_6 and (b) Bi_2WO_6/C-dots/TiO_2. BJH curve displaying pore size distribution of (c) Bi_2WO_6 and (d) Bi_2WO_6/C-dots/TiO_2.

3.2. Photocatalytic activity of z-scheme nano-photocatalyst under solar light illumination.

The photocatalytic efficiency of the synthesized catalysts was tested by observing the decomposition of levofloxacin (fluoroquinolone drug; colorless pollutant). Antibiotic levofloxacin showed the absorbance maximum at λ_{max}=286 nm. Time dependent UV-vis absorbance spectra of the levofloxacin is demonstrated in Fig 6a. The absorbance of the levofloxacin drug solution (10 mg/L)

tend to diminish with increase in reaction time in the existence of the Bi_2WO_6/C-dots/TiO_2 under sunlight. The absolute degradation of the levofloxacin drug was achieved in 90 minutes of sunlight irradiation with 0.075 g/L dose of z-scheme catalyst (Bi_2WO_6/C-dots/TiO_2)' at pH 7 of drug solution (Fig. 6a). Likewise, the degradation of the levofloxacin was monitored without the catalyst, however under solar light illumination, process commonly known as photolysis and there was no degradation observed in the case, thus photolysis proved incompetent for the decomposition of levofloxacin drug (Fig. 6b). However, 28% degradation of drug was obtained with catalyst (0.075 g/L) in 90 minutes under dark conditions (Fig. 6b). Therefore, it came to the revelation that the combination of light and presence of catalyst is mandatory for the efficient degradation of organic contaminants in aqueous medium.

The photocatalytic efficiency of the z-scheme catalyst was also compared with bare Bi_2WO_6 and TiO_2/C-dots under the same augmented and operating conditions. Bi_2WO_6 exhibited 88.3% degradation, whereas TiO_2/C-dots showed 87.24% degradation of levofloxacin with same catalyst dose after 90 minutes of photocatalytic reaction (Fig 6b). The similar percentage of degradation of both the catalysts might be due to their almost similar E_g values calculated from UV-vis DRS studies.

The impact of catalyst dose was studied to optimize the amount of catalyst usage in the photocatalytic reaction. The catalyst (Bi_2WO_6/C-dots/TiO_2) dose was differed from 0.05 g/L to 0.25 g/L, while maintaining critical factors constant, i.e. initial substrate concentration (10 mg/L) and pH of drug solution to be 7 (neutral). Since the catalyst dose was raised from 0.05 g/L to 0.075 g/L, the degradation of levofloxacin was also observed to increase from 97% to 99% with Bi_2WO_6/C-dots/TiO_2, however, the further rise in catalyst dose from 0.075 g/L to 0.1 g/L, resulted in a decrease in the degradation of levofloxacin to 88.7% and at a further increase in catalyst dose to 0.25 g/L, the degradation dropped to 82.58%. It indicated that any further increments in catalyst dose did not bring significant or enhanced degradation. The enhancement in photocatalytic activity with increased catalyst dose is attributed to the accessibility of a greater number of active sites on the surface of the Bi_2WO_6/C-dots/TiO_2 and when catalyst dose was increased above 0.075 g/L, the photocatalytic decomposition of levofloxacin drug decreased because of the shielding effect caused by nanoparticles at increased catalyst doses. This phenomenon explains the masking effect at the surface of the catalyst from illumination, hence obstructing the photons from reaching the substrate (levofloxacin). In other terms, the increased turbidity in the drug solution due to the presence of higher doses of catalyst led to fewer photon penetration and ultimately, the unwanted scattering of photons [36]. The pH of the levofloxacin was also changed from 5 to 9 to optimize the reaction parameters, while maintaining catalyst dose (0.075 g/L) and initial drug concentration of drug solution (10 ppm) constant. The maximum degradation of drug was achieved at neutral pH (7), i.e. 99% and 89.4% and 90% of the degradation was achieved at pH 5 and 9, respectively. The variation in the results might be corresponding to the surface charge of the catalyst.

The initial drug concentration was also varied from 5 mg/L to 20 mg/L. Different concentrations of the drug solution were made by diluting the stock solution (20 mg/L). With the increase in levofloxacin drug concentration, the photocatalytic degradation of drug gradually decreased. The performance of the catalyst was predominantly dependent on the concentration of pollutant. Since, increased concentration of organic pollutant would lead to the reduced formation of oxidizing species and the active sites over the catalyst surface would be captured by drug (substrate), and hence lower degradation [35].

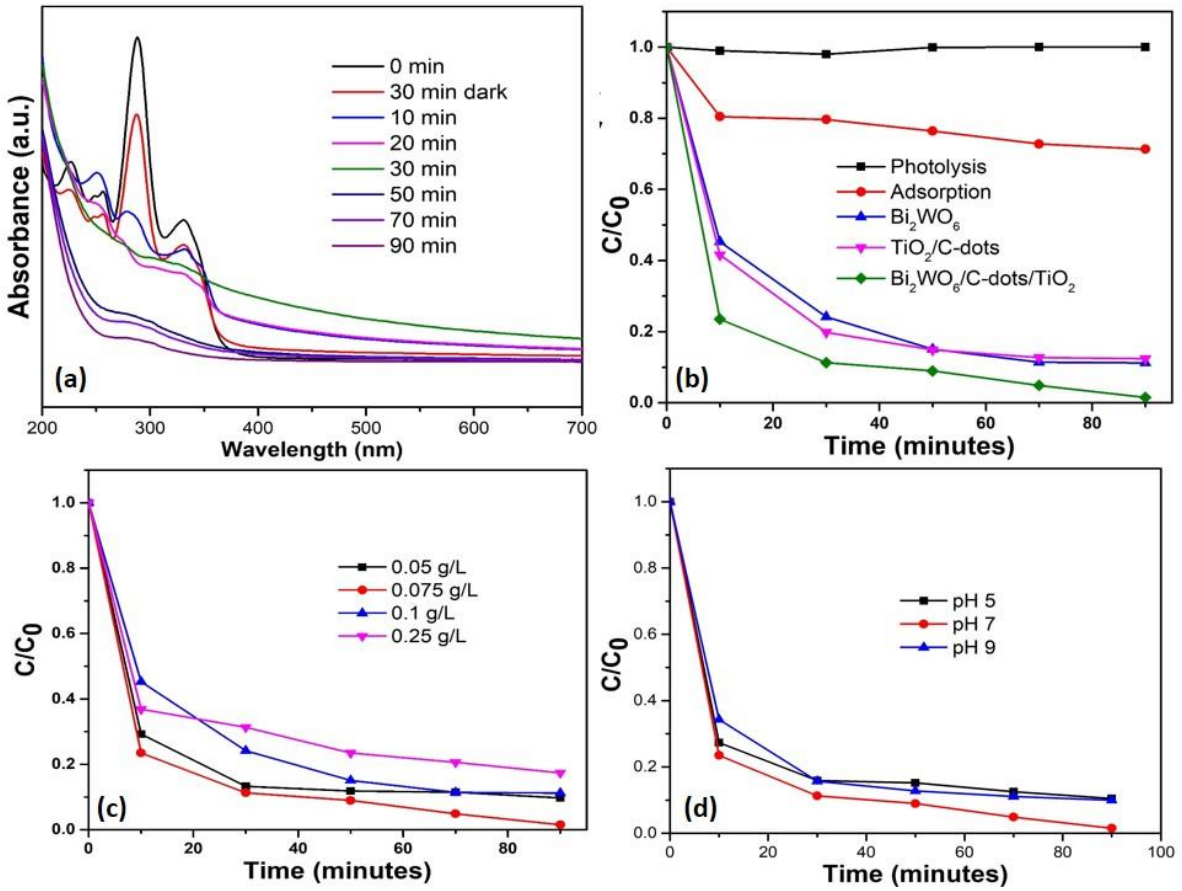

Fig. 6 (a) Time dependent UV-vis absorbance spectra of levofloxacin (10 mg/L, pH 7) under sunlight with Bi_2WO_6/C-dots/TiO_2 (0.075 g/L) (b) Assesment of photolysis, adsorption and photocatalytic efficiency of Bi_2WO_6/C-dots/TiO_2 with bare Bi_2WO_6 and TiO_2/C-dots (catalyst dose 0.075 g/L, pH 7, Conc. of drug 10 mg/L (c) Effect of variation in catalyst dose (Bi_2WO_6/C-dots/TiO_2) on photocatalytic degradation of drug (d) Effect of change in pH of levofloxacin solution on photocatalytic behaviour of Bi_2WO_6/C-dots/TiO_2 (dose 0.075 g/L) under sunlight

The recyclability of the z-scheme catalyst was also carried out to examine its chemical stability for up to 4 cycles. For each consecutive cycle, the catalyst was separated from the reaction mixture by centrifugation, washed thoroughly with mixture of ethanol and distilled water (till the pH of supernatant is neutral) and dried in oven at 80^0C. The percentage degradation of levofloxacin for three cycles was calculated to be 99%, 95% and 92% indicating that the ternary z-scheme catalyst can be used efficiently as a reusable catalyst and thermal and mechanical stability could also be expected.

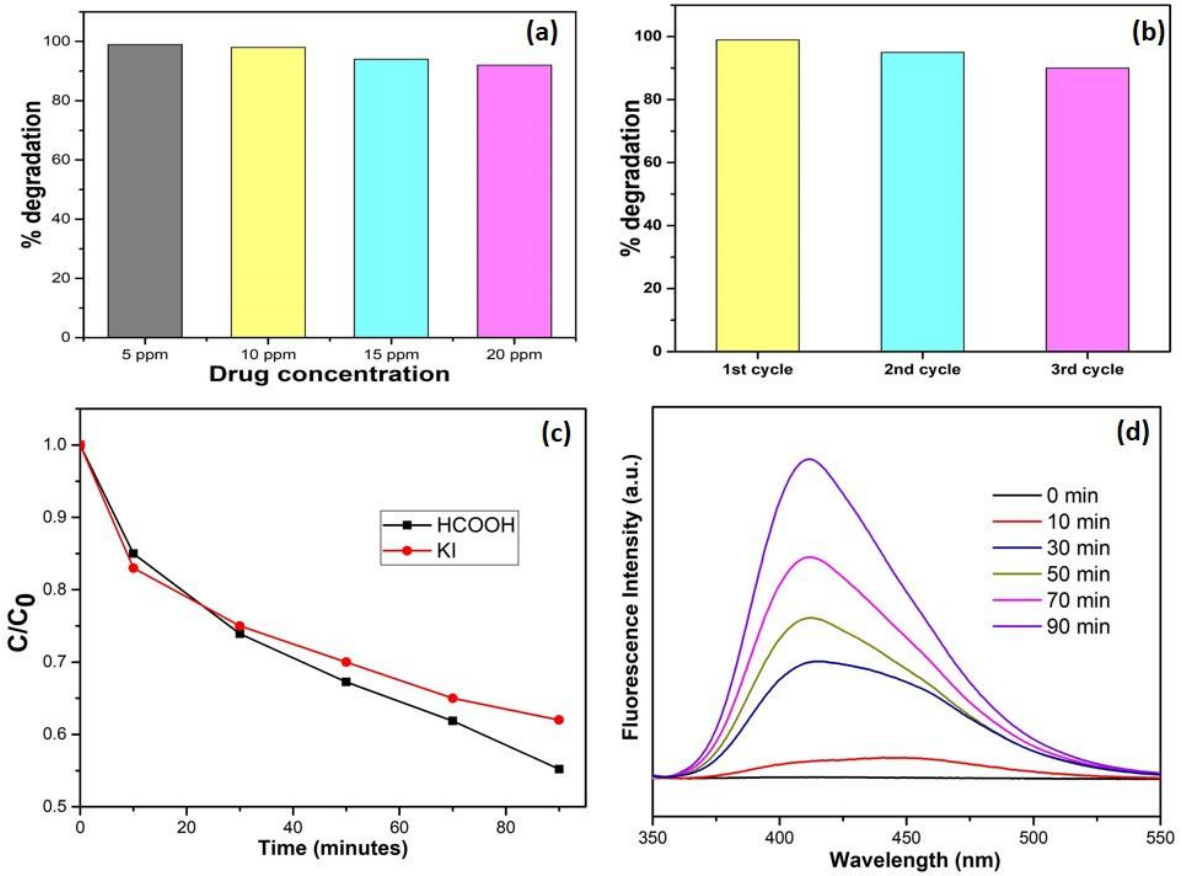

Fig. 7 (a) Influence of initial concentration of drug on the degradation of levofloxacin (b) No. of consecutive runs depicting recyclability of Bi_2WO_6/C-dots/TiO_2 (c) Influence of scavengers on the photocatalytic activity of catalyst (drug conc. 10 ppm, pH 7, catalyst (Bi_2WO_6/C-dots/TiO_2) dosage 0.075 g/L) (d) PL spectra of TPA in presence of catalyst (Bi_2WO_6/C-dots/TiO_2) at λ_{ex}=315 nm.

3.3. Probable mechanism for levofloxacin degradation with z-scheme catalyst under solar light irradiation

The CB and VB potentials of Bi_2WO_6 and TiO_2 were computed from the calculations based on UV-DRS studies and also by employing following equations:

$$E_{VB} = X_e - E_e + 0.5\ E_g$$

$$E_{CB} = E_{VB} - E_g$$

Where E_{VB} and E_{CB} represent the valence and conduction band edge potentials. E_e represents the energy of free electrons on hydrogen scale, i.e. 4.5 eV. E_g calculated from UV- vis DRS studies for Bi_2WO_6, TiO_2/C-dots and Bi_2WO_6/C-dots/TiO_2 are 2.75 eV, 2.87 eV and 2.50 eV, respectively. Further E_{VB} and E_{CB} of Bi_2WO_6 were calculated to 3.2eV and 0.59 eV, and for TiO_2/C-dots, the corresponding values are 2.8 eV and -0.21 eV, respectively. Depending upon the similar energy band gap values of Bi_2WO_6 and TiO_2, two probable charge transfer mechanisms can be derived: traditional type II (double charge transfer) and z-scheme heterojunction (multiple charge transfer) mechanisms. If the transfer mechanism follows the double charge transfer theory, the photoinduced e^+ on the CB of TiO_2 would likely transfer to the CB of Bi_2WO_6 and the h^+ on the VB of Bi_2WO_6 would migrate to the

393 VB of TiO_2 because the VB and CB potentials of Bi_2WO_6 are all lower than that of TiO_2, respectively.
394 However, the e^+ on the CB of Bi_2WO_6 can't reduce O_2 to generate $^{\bullet}O^{2-}$ because the CB potential of
395 Bi_2WO_6 (0.595 eV/vs. NHE) is lower than the standard redox potential of $O_2/^{\bullet}O^{2-}$ (−0.046 eV vs. NHE).
396 Similarly, h^+ on the VB of TiO_2 (2.8 eV vs. NHE) also cannot be efficiently oxidize H_2O to yield •OH
397 owing to the almost same redox potential of H_2O/•OH with 2.73 eV vs. NHE.
398 So in order to completely understand the degradation mechanism of antibiotic drug
399 levofloxacin, multiple charge transfer mechanisms have to be followed. When Bi_2WO_6/C-dots/TiO_2 is
400 illuminated by solar light irradiation, the e^- on CB of Bi_2WO_6 and h^+ on the VB of TiO_2 recombined
401 with itself to form an inner heterojunction, nevertheless, the separated e^- and h^+ aggregate on CB of
402 TiO_2 and VB of Bi_2WO_6, respectively. Meanwhile C-dots on the surface of TiO_2 accept as electron
403 reservoir. Owing to the upconverted photoluminescence of C-dots, longer wavelength light could be
404 converted into 350–650 nm light (shorter wavelength). Then, Bi_2WO_6 and TiO_2, can competently
405 consume the upconverted UV (from C-dots) and visible light, and hence the e^--h^+ pairs were
406 produced on the surface of Bi_2WO_6 and TiO_2. Moreover, due to the z-scheme heterojunction between
407 Bi_2WO_6 and TiO_2, photoinduced e^- in the CB of Bi_2WO_6 moved quickly into the VB of TiO_2 and paired
408 with the h^+, thereby leading to the buildup of e^- in the CB of TiO_2 and h^+ in the VB of Bi_2WO_6. Also,
409 the increased number of e^- in the TiO_2 could be hence moved and gathered within C-dots. Afterwards,
410 the e^- could be reacted to adsorbed O_2 to form superoxide radicals ($O_2^{\bullet-}$). In the meantime, the h^+ in
411 the VB of Bi_2WO_6 could oxidize OH-/H_2O to form ·OH or participate in the degradation of organic
412 pollutants [37,38]. Therefore, it is considered that Bi_2WO_6/C-dots/TiO_2 composite could follow the z-
413 scheme charge transfer mechanism.
414 Scavenger radical studies also confirmed the formation of holes and electrons in the
415 photocatalytic reaction mechanism. The photocatalytic degradation of levofloxacin was observed to
416 significantly decreased from 99% to 43% and 35% in the presence of HCOOH (quencher for electrons)
417 and KI (quencher for holes), respectively (Fig. 7c). Hence, it was proven that the e^- and h^+ have a
418 pivotal part to play in the degradation of levofloxacin. The formation of hydroxyl radicals in the
419 photocatalytic reaction was determined by the TPA fluorescence process. TPA has tendency to
420 transform itself into a fluorescent compound, i.e. 2-hydroxyterephthalic acid, on encountering
421 photogenerated ·OH. So, it is presumed that the production of hydroxyl radical species in the system
422 was proportional to the PL emission intensity of 2-hydroxyterephthalic acid. It could be seen in Fig.
423 7d, that the intensity of PL emission progressively rose under solar light irradiation with z-scheme
424 photocatalyst. Hence, it is suggested that hydroxyl radicals were formed throughout the production
425 of 2-hydroxyterephthalic acid and, thus, have a key role in the degradation of levofloxacin This
426 compound was also observed to support the proposed mechanism of the photocatalytic process. Fig.
427 8 represents the diagrammatic illustration of the photocatalytic degradation mechanism of
428 levofloxacin with Bi_2WO_6/C-dots/TiO_2 under sunlight irradiation.
429

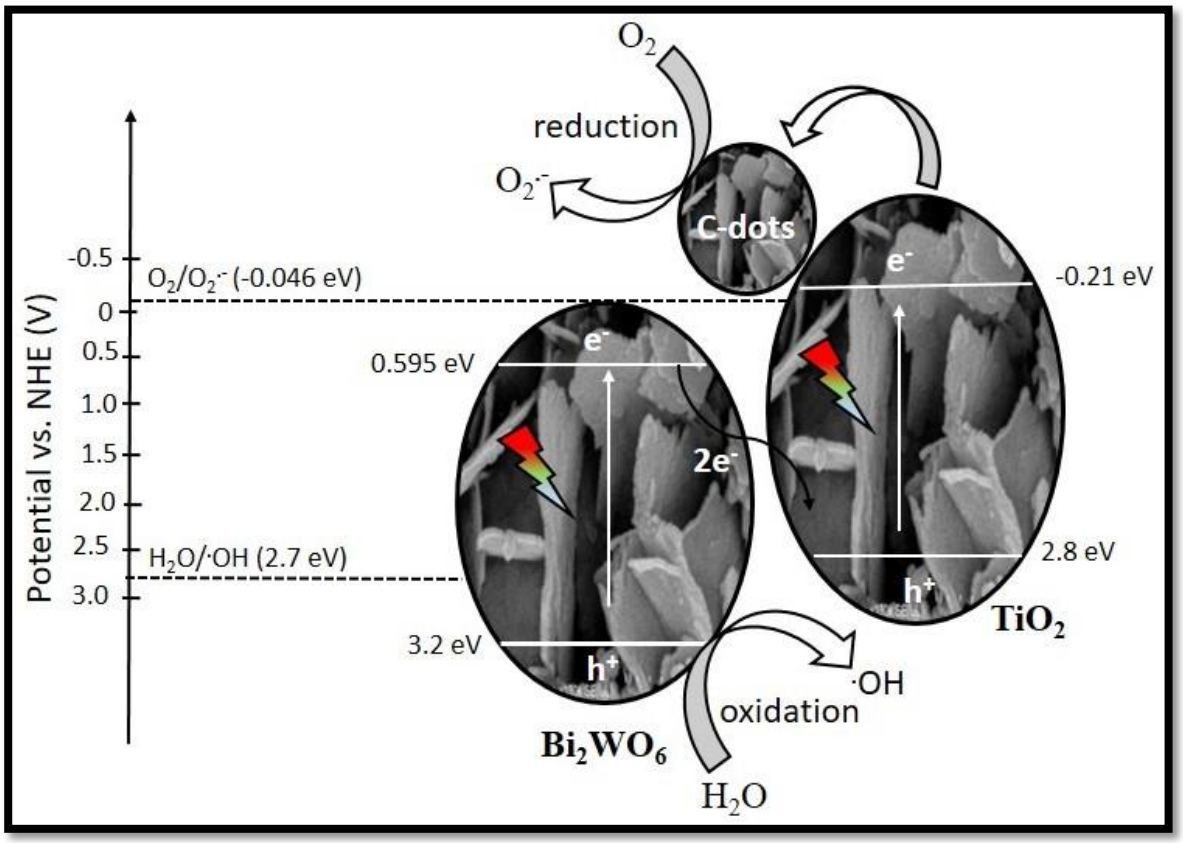

Fig. 8 Plausible mechanism of photocatalytic degradation of levofloxacin with z-scheme photocatalyst.

3.4 Investigation of degradation intermediates formed in the photocatalytic degradation of levofloxacin

Attempts were made to elucidate the reaction intermediates composed during and after the photocatalytic degradation of levofloxacin at different time intervals and the plausible degradation pathway was constructed through identification of the levofloxacin and its derivatives or intermediates from LC-MS analysis based on the consideration of molecular ion peaks $[M+H]^+$. Levofloxacin has the molecular formula (M=361.38 g/mol) according to its chemical formula $C_{18}H_{20}FN_3O_4$, and exhibited a protonated molecular peak at m/z=362 [22]. In addition to the protonated peak of lexofloxacin, fewer intermediates were observed in MS spectra of the levofloxacin samples withdrawn at time periods with the protonated peaks at *m*/*z*=392, 249, 282, 209 and 101, respectively. The mass spectrograms are provided in Fig. S3 of supporting information. The ring-opening or de-methylation at the N1 and N4 position, followed by further oxidation via hydroxyl radicals led to the formation of intermediate at m/z=392 [35]. A fragment at m/z=346 might has been originated from the levofloxacin due to the loss of methyl group ($-CH_3$). The as formed fragment underwent decarboxylation ($-CO_2$) and leading possibly to the formation of another intermediate with m/z of 302. Consequently, with the loss of HF from the former intermediate, another mass fragment at m/z=282 was obtained. A further m/z=249 (intermediate) was formed when an intermediate with m/z=346 underwent a gross loss of moiety $C_5H_{10}N_2$. Likewise, another intermediate at m/z=263 might be obtained by the ring opening of the morpholine moiety at m/z=279 and underwent dehydrations with loss of H_2O, revealed by the presence of the intermediate at

m/z=209 [39]. N-methyl piperazine with m/z value of 101 was derived from the levofloxacin with the cleavage of piperazinyl substituent [40].

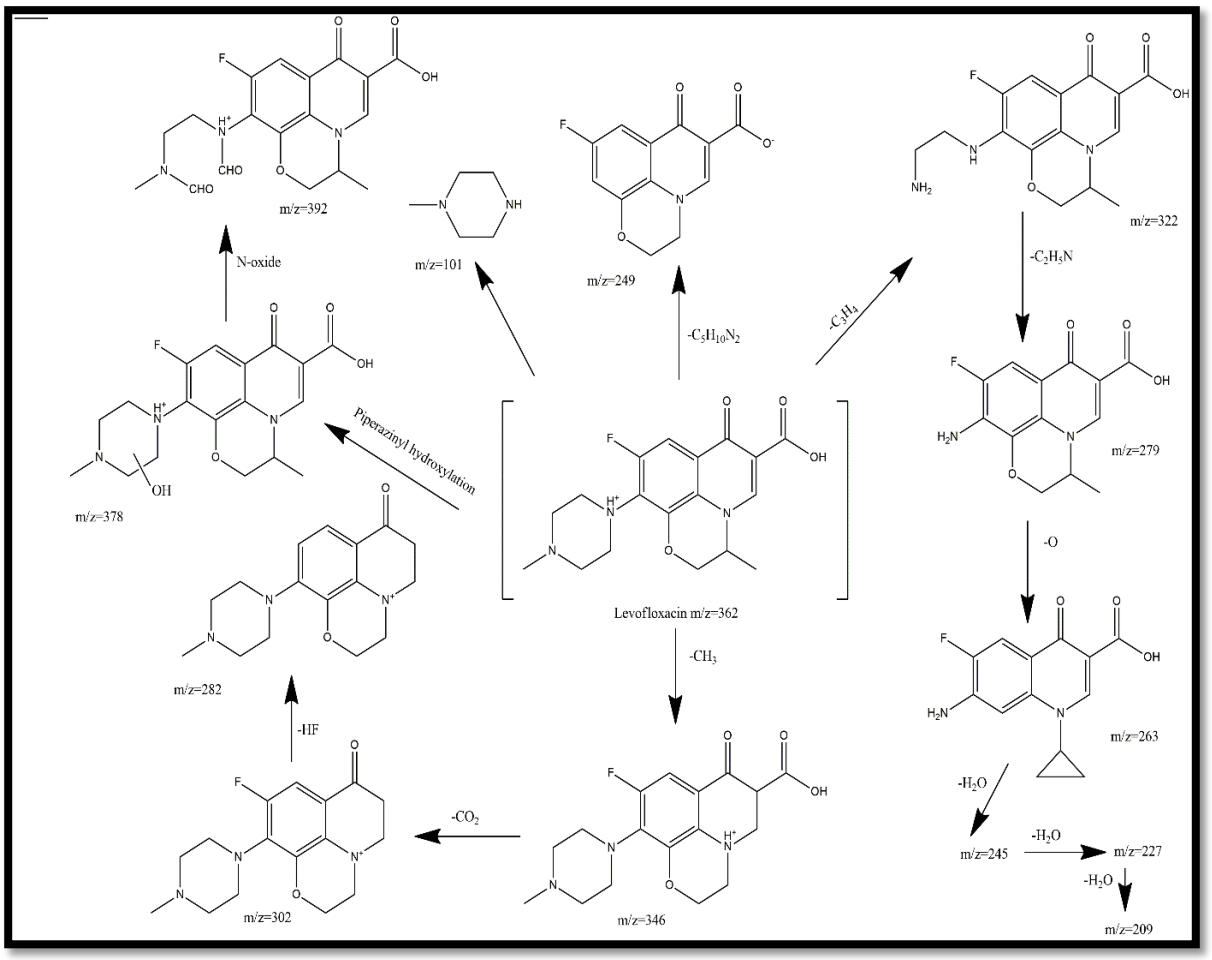

Fig. 9 Identification of degradation intermediates formed during the photocatalytic reaction.

The kinetics of the photocatalytic degradation of levofloxacin was studied by Langmuir Hinshelwood kinetic model using the given equation

$$\ln(C_0/C)=kt$$

where C_0 and C are the initial and final concentration of the drug solution, k is the rate constant and can be calculated from slope of the reaction and t is the time interval of the photocatalytic reaction.

Table 2. Kinetics data of photocatalytic reaction of levofloxacin with different catalysts

S. No.	Photocatalyst	Rate Constant (min^{-1})	R^2
1	Bi_2WO_6/C-dots/TiO_2	0.01831	0.99411
2	Bi_2WO_6	0.01767	0.9977
3	TiO_2/C-dots	0.01713	0.99494

The degradation of drug obeyed pseudo first order kinetics with all photocatalysts with different values of co-relation values (Fig. 10). Other significant details are shown in tabular form (Table 2).

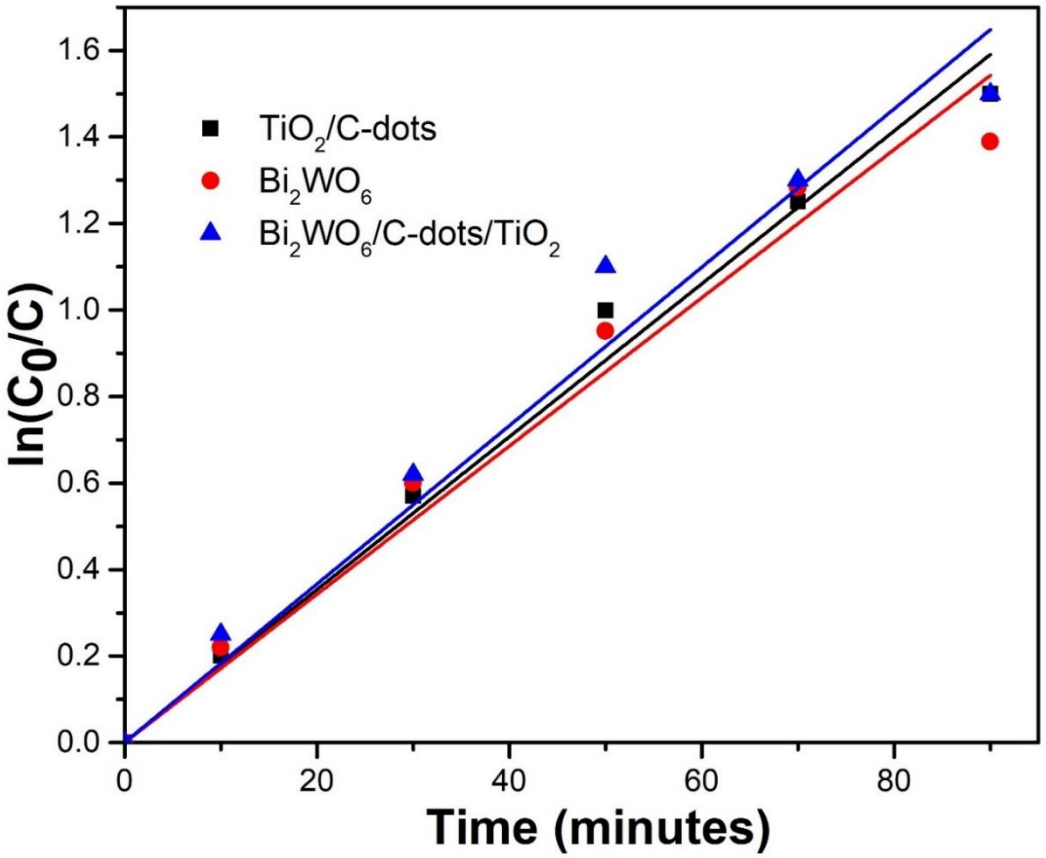

Fig. 10 Graph of ln(C_0/C) against time depicting kinetics of photocatalytic reaction.

4. Conclusions

A novel ternary z-scheme catalyst Bi_2WO_6/C-dots/TiO_2 was successfully fabricated by ultrasonic assisted hydrothermal method and characterized by a number of techniques. The crystallite size of the catalyst was found to be 34.29 nm from powder XRD studies. FESEM images explained that Bi_2WO_6 exhibited nanoflakes like morphology that aggregated to form nanosheets, while nanoparticles of TiO_2/C-dots were found to be assembled over the surface of nanoflakes. PL studies emphasized the optical properties of Bi_2WO_6/C-dots/TiO_2, indicating the hindrance in the recombination of photo-induced charge transporters in z-scheme catalyst over bare Bi_2WO_6, suggesting that z-scheme catalyst could enhance the photocatalytic activity. This hypothesis is supported by UV-DRs studies which showed that the z-scheme catalyst has a lower band gap, i.e. 2.50 eV compared to Bi_2WO_6 (2.75 eV) and TiO_2/C-dots (2.87 eV). This suggests that Bi2WO6/C-dots/TiO_2 can be considered as efficient potential photocatalyst in the visible region of the solar spectrum. The photocatalytic behaviour of the synthesized catalysts was investigated by monitoring the degradation of fluoroquinolone levofloxacin drug under 90 minutes of sunlight illumination. Almost complete degradation was observed with Bi_2WO_6/C-dots/TiO_2, whereas 88.3% and 87.24% degradation with Bi_2WO_6 and TiO_2/C-dots under similar reaction conditions. The higher specific surface area of Bi_2WO_6/C-dots/TiO_2 compared to bare Bi_2WO_6 calculated from nitrogen adsorption desorption isotherm, also showed that the z-scheme catalyst would provide more surface for the adsorption of the drug molecules and hence, improved photocatalytic activity. Experimental

parameters including catalyst dose, reaction time, pH of drug solution and initial drug concentration were studied to optimize the photocatalytic reaction. A plausible mechanism for the degradation of the drug was also proposed based on scavenger radical trap experiments and TPA fluorescence technique. LC-MS analysis showed intermediates and other products at different stages of the photocatalytic process.

Supplementary Materials: The following are available online at www.mdpi.com/xxx/s1, Figure S1: (a,b,c) FESEM images of Bi_2WO_6 at different magnifications. (d) EDS spectrum of Bi_2WO_6; Figure S2: TEM image of TiO_2/C-dots; Figure S3: Mass spectrographs of levofloxacin drug at different time intervals of photocatalytic reaction; Table S1: Elemental composition of Bi_2WO_6

Author Contributions: "Conceptualization, S.S., S.K.K and A.U.; methodology, S.S; software, S.S.; validation, X.X., A.O.I., M.G.F., S.K.M, S.E, S.K.K. and A.U; formal analysis, S.S.; investigation, S.S.; resources, S.S.; data curation, S.S., S.K.K, A.U.; writing—original draft preparation, S.S., S.K.K, A.U.

Funding: UGC–BSR, Government of India is acknowledged for providing financial support through the grant no. F. 25-1/2013(BSR)/5-91/2007(BSR).

Acknowledgments: Shelja Sharma thanks UGC–BSR Government of India for providing financial support through the grant no. F. 25-1/2013(BSR)/5-91/2007(BSR) and Department of Biotechnology, Government of India and British Council, United Kingdom for the award of Newton-Bhabha PhD Placement.

Conflicts of Interest: The authors declare no conflict of interest.

References

1. Sorensen, B.H.; Nielsen, N., Lanzky, P.F., Ingerslev, F., Holten Lutzhoft, H.C., Jorgensen, S.E. Occurrence fate and effects of pharmaceutical substances in the environment- a review. *Chemosphere* **1988**, *36(2),* 357-393.
2. Abellan, M.N.; Gimenez, J.; Esplugas, S. Photocatalytic degradation of antibiotics: The case of sulfamethoxazole and trimethoprim. *Catal. Today* **2009**, *144(1-2),* 131-136.
3. Hignite, C.; Azarnoff, D.L.; Drugs and drug metabolites as environmental contaminants: chlorophenoxyisobutyrate and salicyclic acid in sewage water effluent. *Life Sci.* **1977**, *20 (2)*, 337-341.
4. Chen, M.; Chu, W. Photocatalytic degradation and decomposition mechanism of fluoroquinolones norfloxacin over bismuth tungstate: Experiment and mathematic model. *Appl. Catal., B* **2015**, *168–169*, 175–182
5. Najjar, N.H.E.; Touffet, A.; Deborde, M.; Journal R.; Leitner, N.K.V. Levofloxacin oxidation by ozone and hydroxyl radicals: kinetic study, transformation products and toxicity. *Chemosphere* **2013**, *93*, 604–611.
6. Epold, I.; Trapido, M. Dulova, N. Degradation of levofloxacin in aqueous solutions by Fenton, ferrous ionactivated persulfate and combined Fenton/persulfate systems. *Chem. Eng. J.* **2015**, *279*, 452–462.
7. Ge, L.; Na, G.; Zhang, S.; Li, K.; Zhang, P.; Ren, H.; Yao, Z. New insights into the aquatic photochemistry of fluoroquinolone antibiotics: Direct photodegradation, hydroxyl-radical oxidation, and antibacterial activity changes. *Sci. Total Environ*. **2015**, *527–528*, 12–17
8. Chen, M.; Chu, W. Degradation of antibiotic norfloxacin in aqueous solution by visible-light-mediated C-TiO2 photocatalysis. *J. Hazard. Mater.* **2012**, *219–220*, 183–189.
9. Oberle, K.; Capdeville, M.J.; Berthe, T.; Budzinski, H.; Petit, F. Evidence for a complex relationship between antibiotics and antibiotic-resistant Escherichia coli; from medical center patients to a receiving environment. *Environ. Sci. Technol.* **2012**, *46*, 1859-1868.
10. Sharma, S.; Mehta, S.K.; Kansal, S.K. N doped ZnO/C-dots nanoflowers as visible light driven photocatalyst for the degradation of malachite green dye in aqueous phase. *J. Alloys Compd.* **2017**, *699*, 323–333.
11. Kaur, A.; Umar, A.; Kansal, S.K. Sunlight-driven photocatalytic degradation of non-steroidal anti-inflammatory drug based on TiO_2 quantum dots. *J. Colloid Interface Sci.* **2015**, *459*, 257–263.
12. Xiang, Q.J.; Yu, J.G.; Jaroniec, M. Synergetic Effect of MoS_2 and graphene as cocatalysts for enhanced photocatalytic H_2 production activity of TiO_2 nanoparticles. *J. Am. Chem. Soc*. **2012**, *134*, 6575 .

13. Christians, J.A.; Fung, R.C.M.; Kamat, P.V. An inorganic hole conductor for organo-lead halide perovskite solar cells. improved hole conductivity with copper iodide. *J. Am. Chem. Soc*. **2014** ,*136*, 758.

14. Kondratenko, E.V.; Mul, G.; Baltrusaitis, J.; Larrazábal, G.O., Pérez-Ramírez, J. Status and perspectives of CO_2 conversion into fuels and chemicals by catalytic, photocatalytic and electrocatalytic processes. *Energy Environ. Sci*. **2013**, *6*, 3112.

15. Roy, S.C.; Varghese, O.K.; Paulose, M.; Grimes, C.A. Toward solar fuels: photocatalytic conversion of carbon dioxide to hydrocarbons. *ACS Nano* **2010**, *4*, 1259.

16. Dhakshinamoorthy, A.; Navalon, S., Corma, A.; Garcia, H. Photocatalytic CO_2 reduction by TiO_2 and related titanium containing solids, *Energy Environ. Sc*i. **2012**, *5*, 9217

17. Formal, F.L.; Pendlebury, S.R.; Cornuz, M.; Tilley, S.D.; Grä tzel, M.; Durrant, J.R. Back electron–hole recombination in hematite photoanodes for water splitting. *J. Am. Chem. Soc.* **2014**, *136*, 2564 .

18. Li, X.H.; Antonietti, M. Metal nanoparticles at mesoporous N-doped carbons and carbon nitrides: functional Mott-Schottky heterojunctions for catalysis. *Chem. Soc. Rev.* **2013**, *42*, 6593 .

19. Kumar, S.G.; Rao, K.S.R.K.; Physics and chemistry of CdTe/CdS thin film heterojunction photovoltaic devices: fundamental and critical aspects. *Energy Environ. Sci*. **2014**, *7*, 45

20. Sayama, K.; Mukasa, K.; Abe, R.; Abe, Y.; Arakawa, H. A new photocatalytic water splitting system under visible light irradiation mimicking a Z-scheme mechanism in photosynthesis. *J. Photoch. Photobio. A* **2002**, *148*, 71 .

21. Sayama, K.; Mukasa, K.; Abe, R.; Abe, Y.; Arakawa, H. Stoichiometric water splitting into H_2 and O_2 using a mixture of two different photocatalysts and an IO_3^-/I^- shuttle redox mediator under visible light irradiation. *Chem. Commun*. **2001**, 2416.

22. Sharma, S.; Umar, A.; Mehta, S.K.; Ibhadon, A.O.; Kansal, S.K. Solar light driven photocatalytic degradation of levofloxacin using TiO_2/carbon-dot nanocomposites. *New J. Chem.* **2018**, *42*, 7445.

23. Wang, W.; Ni, Y., Xu, Z. One-step uniformly hybrid carbon quantum dots with high-reactive TiO2 for photocatalytic application. *J. Alloys Compd*. **2015**, *622*, 303–308.

24. Liu, R.; Li, H.; Duan, L.; Shen, H.; Zhang Y.; Zhao, X. In situ synthesis and enhanced visible light photocatalytic activity of C-TiO_2 microspheres/carbon quantum dots. *Ceram. Int.* **2017**, *43*, 8648–8654.

25. Di, J.; Xia, J.; Ge, Y.; Li, H.; Ji, H.; Xu, H.; Zhang, Q. Novel visible-light-driven CQDs/ Bi_2WO_6 hybrid materials with enhanced photocatalytic activity toward organic pollutants degradation and mechanism insight. *Appl. Catal. B: Environ*. **2015,** *168–169*, 51–61.

26. Wu, Q.S.; Feng, Y.; Zhang, G.Y.; Sun, Y.Q.; Xu, Y.Y.; Gao, D.Z. a-Fe_2O_3 modified Bi_2WO_6 flower-like mesostructures with enhanced photocatalytic performance. *Mater. Res. Bull.* **2014,** *49,* 440–447.

27. Wang, T.; Zhang, F.; Xiao, G.; Zhong, S; Lu, C. Synthesis of Bi2WO6/Bi2O3 composite with enhanced photocatalytic activity by a facile one-step hydrothermal synthesis route. *Photochem. Photobiol.* **2015,** *91,* 291–297.

28. Kumar, V.; Prasad, M.D.; Vithal, M. Enhanced visible light photocatalytic activity of Sn doped Bi_2WO_6 nanocrystals. *Mater. Lett.* **2015,** *152,* 200–202.

29. Xia, J.; Li, H.; Luo, Z.; Xu, H.; Wang, K.; Yin, S.; Yan, Y. Self-assembly and enhanced optical absorption of Bi2WO6 nest via ionic liquid-assisted hydrothermal method. *Mater. Chem. Phys.* **2010,** *121,* 6–9.

30. Cao, R.; Huang, H.; Tian, N.; Zhang, Y., Guo, Y.; Zhang, T. Noval Y doped Bi2WO6 photocatalyst: Hydrothermal fabrication, characterization and enhanced visible-light-driven photocatalytic activity for rhodamine B degradation and photocurrent generation. *Mater. Charact.* **2015,** *101,* 166–172.

31. Phuruangrat, A.; Dumrongrojthanath, P.; Ekthammathat, N.; Thongtem, S.; Thongtem, T. Hydrothermal synthesis, characterization and visible light-driven photocatalytic properties of Bi2WO6 nanoplates. *J. Nanomater.* **2014** 1–7. Article id 138561.

32. Wang, Y.; Bai, X., Pan, C.; He, J.; Zhu, Y. Enhancement of photocatalytic activity of Bi2WO6 hybridized with graphite-like C_3N_4. *J. Mater. Chem*. **2012**, *22*, 11568–11573.

33. Min, Y.; Zhang, K.; Chen, Y.; Zhang, Y.; Zhao, W. Synthesis of nanostructured ZnO/ Bi2WO6 heterojunction for photocatalysis application. *Sep. Purif. Technol*. **2012**, *92*, 115–120.

34. Xiao, Q.; Zhang, J.; Xiao, C.; Tan, X. Photocatalytic degradation of methylene blue over Co3O4/Bi2WO6 composite under visible light irradiation. *Catal. Commun*. **2008**, *9*, 1247–1253.

35. Hapeshi, E.; Fotiou, I.; Fatta-Kassinos, D. Sonophotocatalytic treatment of ofloxacin in secondary treated effluent and elucidation of its transformation products. *Chem. Eng. J.* **2013**, *224*, 96–105.

36. Li, H.T.; He, X.D.; Kang, Z.H.; Huang, H.; Liu, Y.; Liu, J.L.; Lian, S.Y; Tsang, C.H.A.; Yang, X.B.; Lee, S.T. Water-soluble fluorescent carbon quantum dots and photocatalyst design. *Angew. Chem., Int. Ed.* **2010**, *49*, 4430–4434.

600 **37.** Hapeshi, E.; Achilleos, A.; Vasquez, M.I.; Michael, C.; Xekoukoulotakis, N.P.; Mantzavinos, D.; Kassinos,
601 D. Drugs degrading photocatalytically: Kinetics and mechanisms of ofloxacin and atenolol removal on
602 titania suspensions. *Water Res.* **2010**, *44*, 1737–1746.
603 **38.** Xie, Z.; Feng, Y.; Wang, F.; Chen, D.; Zhang, Q.; Zeng, Y.; Lv, W; Liu, G. Construction of carbon dots
604 modified MoO_3/g-C_3N_4 Z-scheme photocatalyst with enhanced visible-light photocatalytic activity for the
605 degradation of tetracycline. *Appl. Catal. B.* **2018**, *229*, 96-104.
606 **39.** Wang, L.; Zhao, Q.; Hou, J.; Yan, J.; Zhang, F.; Zhao, J.; Ding, H.; Li, Y. Ding, L.; One-step solvothermal
607 synthesis of magnetic Fe_3O_4-graphite composite for Fenton-like degradation of levofloxacin. *J. Environ. Sci.*
608 *Health., Part A.* **2016**, *51*, 52–62.
609 **40.** Kaur, A.; Salunke, D.B.; Umar, A.; Mehta, S.K.; Sinha, A.S.K.; Kansal, S.K. Visible light driven
610 photocatalytic degradation of fluoroquinolone levofloxacin drug using Ag2O/TiO2 quantum dots: a
611 mechanistic study and degradation pathway. *New J.Chem.* **2017**, *41*, 12079-12090.
612

613